ELSEVIER

Catalysis Today 68 (2001) 21–30

CATALYSIS TODAY

www.elsevier.com/locate/cattod

Comparative study of nanocrystalline zirconia prepared by precipitation and sol–gel methods

J.A. Wang [a,*], M.A. Valenzuela [a], J. Salmones [b], A. Vázquez [b], A. García-Ruiz [c], X. Bokhimi [d]

[a] *Laboratory of Catalysis and Materials, Superior School of Chemical Engineering (ESIQIE), National Politecnic Institute (IPN), Zacatenco, 07738 Mexico City, Mexico*

[b] *Institute of Mexican Petroleum, Eje Central Lázaro Cárdenas 152, 07730 Mexico City, Mexico*

[c] *UPIICSA, National Polytechnic Institute, Té No. 950 Esq. Resina, 08400 Mexico City, Mexico*

[d] *Institute of Physics, National University of Mexico (UNAM), A.P. 20-364, 01000 Mexico City, Mexico*

Abstract

The crystalline properties of zirconia synthesized by the precipitation and sol–gel methods were comparatively studied. Samples were characterized with thermoanalysis and X-ray powder diffraction techniques. The tetragonal and monoclinic crystalline structures of zirconia were refined with the Rietveld technique, which provided the quantitative information concerning the lattice cell parameters, phase concentrations, average crystallite sizes and the concentrations of the cationic and anionic vacancies. Both synthesis methods gave rise to nanocrystalline zirconia. The samples calcined at 800°C and prepared by the precipitation had average crystallite sizes less than 18 nm, which were two times smaller than the corresponding values obtained in the sol–gel samples. Both tetragonal and monoclinic nanocrystalline phases had atomic defects in concentrations that depended on the synthesis method and annealing temperature.

Keywords: Zirconia crystalline structure refinement; Sol–gel synthesis; Precipitation synthesis; Lattice vacancies; Nanocrystalline zirconia

1. Introduction

Over the last 10 years, the zirconia used as catalyst or catalytic support has attracted much attention [1–5]. When it is doped with sulfuric acid or ammonium sulfate, as reported by Arata and Hino [6–8], zirconia exhibits an acidity 10^4 times stronger than 100% sulfuric acid characterized by Hammett acid function, therefore it is recognized as a *superacid*. Because this discovery, numerous studies have been devoted to the synthesis of sulfated zirconia, aiming to develop new catalytic processes [9–13]. Due to its strong acidity, sulfated zirconia is believed to be a potential catalyst for isomerization at relatively low temperatures, as it has been shown for light alkanes [14–16].

Since zirconia has a lattice with many vacancies, it is a good ionic conductor at high temperatures. These vacancies allowed it to be used as an oxygen sensor to measure the air-to-fuel ratio in internal combustion engines in order to control the emissions of NO_x, CO and hydrocarbon compounds [17]. The above zirconia property is also used in oxygen pumps [18,19], solid oxide fuel cells and electrolysis [20].

Although the crystalline structure of zirconia phases has been studied for many years, a quantitative determination of its defect concentration has not been reported in the open publications [21–24]. From the viewpoint of catalysis, the determination of structural

* Corresponding author. Tel.: +52-5-726000, ext: 55124; fax: +52-5-682728.
E-mail address: wang_j_a@yahoo.com (J.A. Wang).

0920-5861/01/$ – see front matter
PII: S0920-5861(01)00319-4

defects is of important since these defects are usually acted as catalytic active sites involving in many catalysis reactions.

The crystalline structures and catalytic properties of zirconia are generally dependent of its synthesis method and thermal treatment. In general, zirconia can be synthesized by using different methods, from them, the traditional precipitation technique may give rise to microcrystalline zirconia; the sol–gel method, however, produces nanocrystalline zirconia, which is very attractive for novel applications, because nanocrystalline structures often exhibit properties different from those observed in microcrystalline structures.

Zirconia has three stable crystalline phases: tetragonal, monoclinic and cubic zirconia. Their concentrations and transformation between each other depend on zirconia doping and its thermal treatment. This, when it is used as catalyst support or catalyst, affects its catalytic properties.

The aim of the present work is to study the crystalline structures of two kinds of zirconia sample sets: one prepared by using the precipitation technique, and the other by using the sol–gel method. Thermal decomposition and phase transformation of the samples were characterized with thermogravimetric analysis (TG–DTG), differential thermal analysis (DTA), and X-ray powder diffraction (XRD) techniques. The crystalline structures of the samples calcined at different temperatures were refined via Rietveld technique, which provided quantitative information concerning the cationic and anionic defects in the crystalline structures, lattice parameters and phase concentrations.

2. Experimental

2.1. Sample preparation

2.1.1. Precipitation method

A solution of 13.07 g of zirconyl chloride ($ZrOCl_2 \cdot 8H_2O$) in 500 ml of water was dropped into a recipient containing 300 ml of water. While the solution was stirred, a solution of 0.1 M ammonia was dropwise added to it until reaching pH 10. This alkaline solution was continuously stirred for 1 h, and then aged for 24 h until forming a precipitate, which was washed several times with distilled water. The precipitate was dried at 120°C for 4 h to obtain the fresh sample, which was annealed in air at 400, 600 and 800°C for 4 h.

2.1.2. Sol–gel method

Zirconium *n*-butoxide (11 ml) was dissolved into 35.2 ml of absolute ethanol under continuous stirring. To the homogeneous solution was dropped the hydrolysis catalyst (NH_4OH) until reaching pH 10. Thereafter, 2 ml of water were dropped, and the new solution was stirred continuously until gelling. The gel was dried at room temperature in a vacuum for 24 h. Samples was annealed for 4 h in air at 400, 600 and 800°C.

2.2. DTA and TG–DTG analyses

DTA and TG–DTG sample analyses were carried out in air with a Dupont Model 950 thermoanalyzer, in the temperature range between 25 and 1000°C at a heating rate of 20°C/min.

2.3. X-ray diffraction and Rietveld refinements

X-ray diffraction data were measured at room temperature in a Bruker Advance D-8 diffractometer with Cu Kα radiation and a graphite secondary beam monochromator. Intensities were obtained in the 2θ range between 20 and 110° with a step of 0.02° and a measuring time of 2.7 s per point. Crystalline structures were refined using DBWS-9006 PC and WYRIET programs. The tetragonal structure was refined with a tetragonal unit cell with the symmetry described by space group $P4_2/nmc$. The atomic fractional coordinates are reported in Table 1. For refining the crystalline structure of the monoclinic phase its symmetry was described by space group $P2_1/c$, its atomic fractional coordinates are reported in Table 2 and the limits of the these parameters in Table 3. The Rietveld refinement provided not only the concentration and

Table 1
Atomic fractional coordinates of tetragonal zirconia (space group $P4_2/nmc$)

Atom	Site	*x*	*y*	*z*
Zr	2a	0.75	0.25	0.75
O	4d	0.25	0.25	*u*[a]

[a] $0.045 < u < 0.050$.

Table 2
Atomic fractional coordinates of monoclinic zirconia (space group $P2_1/c$)

Atom	Site	x	y	z
Zr	4e	u_x	u_y	u_z
O(1)	4e	v_x	v_y	v_z
O(2)	4e	w_x	w_y	w_z

Table 3
Limits of the fractional coordinates of monoclinic zirconia

Fractional coordinate	Lower limit	Upper limit
u_x	0.2744 (4)	0.280 (2)
u_y	0.038 (2)	0.0421 (6)
u_z	0.2090 (4)	0.226 (2)
v_x	0.040 (3)	0.083 (2)
v_y	0.316 (2)	0.395 (4)
v_z	0.277 (3)	0.347 (1)
w_x	0.438 (2)	0.510 (3)
w_y	0.749 (2)	0.764 (1)
w_z	0.434 (4)	0.503 (3)

average crystallite sizes of each phase in the sample but also the lattice point defects in the crystalline structures. The standard deviations, showing the variation of the last figures of the corresponding number, are given in parentheses. When the numbers corresponded to parameters obtained from the Rietveld refinement, the estimated standard deviations are not estimates of the analysis as a whole but only of the minimum possible errors based on their normal distribution.

3. Results and discussion

3.1. Thermal analyses

Fig. 1 shows the TG–DTG profile of the sample prepared by precipitation method. Three weight loss stages were observed. The largest one located at a 72°C, corresponded to the evaporation of residual ammonia and water adsorbed in the sample. Because it was synthesized in a basic media with pH 10, zirconium hydroxide crystals (referred as $Zr(OH)_4$) were formed during the hydrolysis procedure, which was decomposed when the annealing temperature was increased. The weight loss observed between 200 and 400°C, and the broad endothermic peak registered in the DTA analysis (Fig. 2) corresponded to the decomposition of $Zr(OH)_4$ into ZrO_2.

The small peak at 470°C in the TG curve, and the corresponding sharp peak at the same temperature in the DTA curve are indicative of an additional phase coexisting with zirconia. Based on the XRD analysis which will be shown in the following section, we ascribed this phase to a quasi-amorphous tetragonal phase produced in the decomposition process of $Zr(OH)_4$.

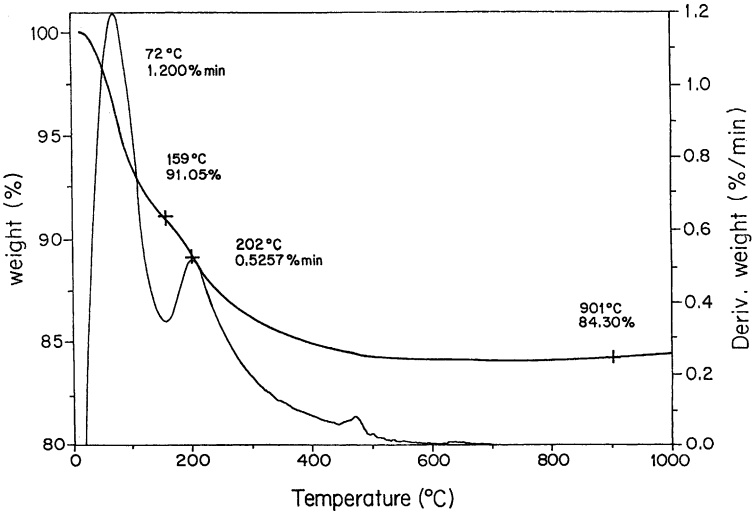

Fig. 1. TG–DTG profiles of the sample prepared with precipitation technique.

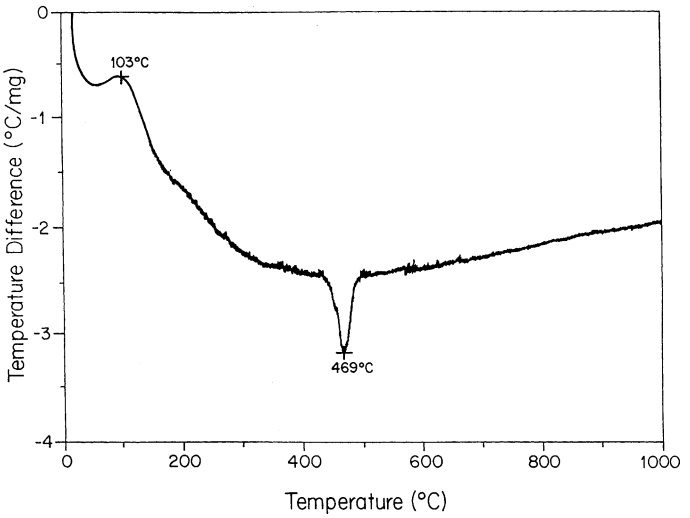

Fig. 2. DTA profile of the sample prepared with precipitation technique.

When the samples were annealed above 600°C, no further weight loss was observed. In the DTA curve, however, the shift of the base line shows that thermal energy was produced during the calcination, which corresponds to transformation from the tetragonal into the monoclinic phase, as shown by the XRD analysis.

The TG–DTG curves (Fig. 3) of the sol–gel sample also had three weight loss stages, while its DTA curve had three peaks (Fig. 4). The origin of these stages and peaks are similar to the explanation for the respective curves of the precipitation sample shown in Figs. 1 and 2. More discussion concerning these assignments will be shown in the section of XRD analysis.

The above decomposition processes can be expressed with the following reactions:

Below 200°C,

$$ZrOCl_2 \cdot 8H_2O + 2NH_4OH \rightarrow Zr(OH)_4 + 2NH_4Cl + 7H_2O \quad (1)$$

200–400°C,

$$2Zr(OH)_4 \rightarrow ZrO_2(t) + ZrO_2(m) + 4H_2O \quad (2)$$

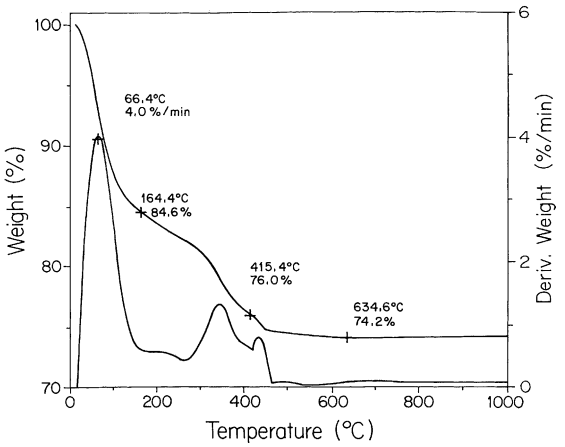

Fig. 3. TG–DTG profiles of the sample prepared with sol–gel technique.

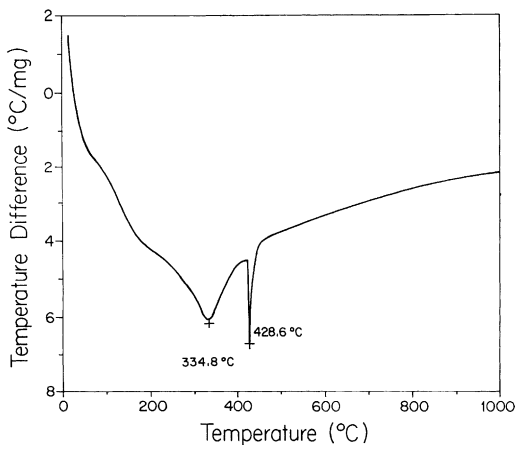

Fig. 4. DTA profile of the sample prepared with sol–gel technique.

$$Zr(OH)_4 \rightarrow \text{quasi-}ZrO_2(t) + 2H_2O \quad (3)$$

400–500°C,

$$\text{Quasi-}ZrO_2(t) \rightarrow ZrO_2(t) \quad (4)$$

above 600°C,

$$ZrO_2(t) \rightarrow ZrO_2(m) \quad (5)$$

In a previous report [23], it is shown that for samples of zirconia prepared by sol–gel using H_2SO_4 as hydrolysis catalyst, the largest decomposition rate of $Zr(OH)_4$ is located at 650°C in the TG curves, which means that ZrO_2 crystallization in acidic media occurred at higher temperature; there are 200°C more than that for the precipitation and sol–gel sample prepared in a base media. This is because the phase transformation from $Zr(OH)_4$ to ZrO_2 involves several possible steps: the loss of the loose water and terminal hydroxyl groups, oxolation of hydroxyl bridges to form embryonic oxide nuclei and growth of the nuclei to form observable crystallites. When the sulfuric acid was used as hydrolysis catalyst, the SO_4^{2-} ions present in the Zr–O framework would replace for OH^- ions. Because the thermal stability of the sulfate to zirconium linkages is much higher than that of the hydroxyl bridges across two Zr atoms, the removal of SO_4^{2-} ions needs a higher temperature, i.e., 600°C, which delays the formation of some oxo bonds and thus stabilizes the low-temperature structure.

3.2. Lattice cell parameters, phase concentration and crystallite size

The XRD patterns of precipitation and sol–gel samples annealed at 400, 600 and 800°C are comparatively shown in Figs. 5 and 6. The Rietveld refinement plots are shown in Figs. 7–10. The lattice cell parameters of tetragonal and monoclinic crystalline structures in sol–gel and precipitation samples, obtained from their refinements, are reported in Tables 4 and 5.

In the crystalline structure of monoclinic, the values of the lattice parameters in *a* and *b* directions of sol–gel sample were a little bit larger than in the precipitated one. When the calcination temperature increased, in both sol–gel and precipitation samples, the unit cell of monoclinic showed a distortion because it expanded in *c* dimension with a contraction in *a* direction. The

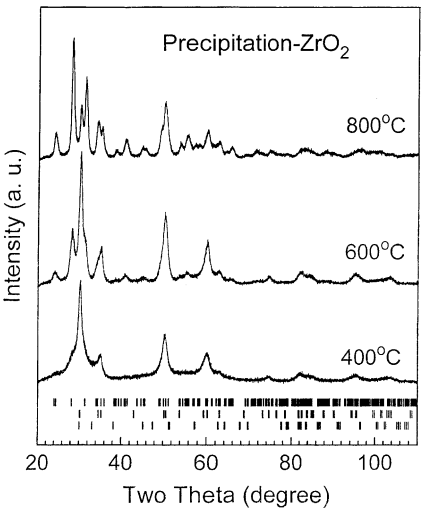

Fig. 5. XRD pattern of the precipitative sample calcined at 400, 600 and 800°C. The upper line marks correspond to tetragonal phase; the middle line marks correspond to a quasi-amorphous tetragonal phase and the lower ones correspond to monoclinic phase.

lattice cell distortion is usually caused by the guest ions like OH^- inserting in the crystalline structure and the calcination temperature. The foreign ions with different radius or charges produce charge unbalance in the locate structure and the calcination temperature

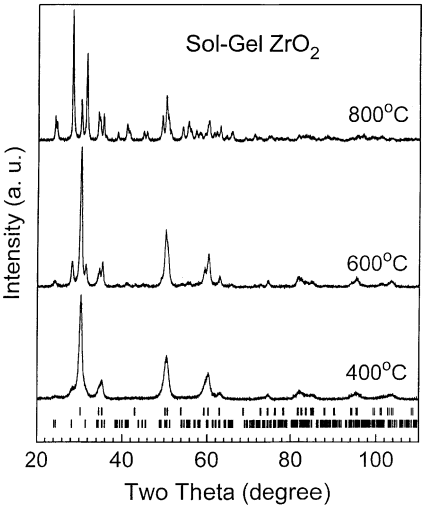

Fig. 6. XRD pattern of the sol–gel sample calcined at 400, 600 and 800°C. The upper line marks correspond to tetragonal phase and the lower line marks correspond to monoclinic phase.

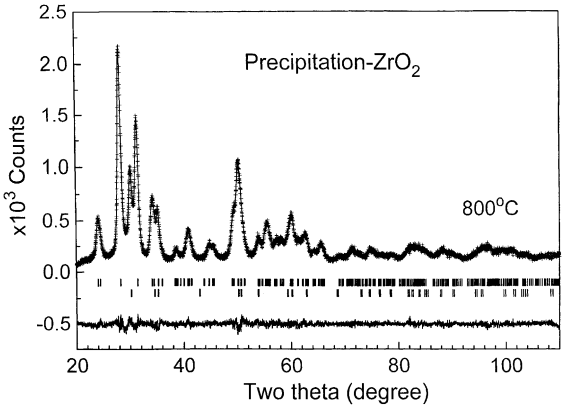

Fig. 7. Rietveld refinement plot of the precipitation zirconia sample calcined at 800°C. The solid continuous line is the calculated pattern while the crosses are the experimental data. The upper line marks correspond to tetragonal phase and the lower line marks correspond to monoclinic phase. The lowest line is the difference between the calculated and experimental data.

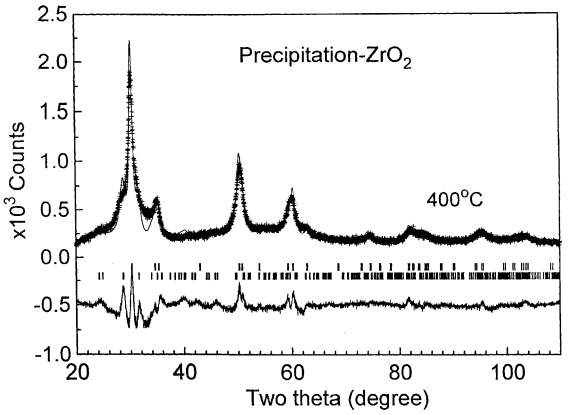

Fig. 9. Rietveld refinement plot of the precipitation zirconia sample calcined at 400°C. The experimental data were fitted with two phases. The upper line marks correspond to tetragonal phase and the lower line marks correspond to monoclinic phase.

may affect the behavior of lattice sites vibration, those factors, in turn, lead to the lattice cell modification in comparison with the ideal crystalline structure. The dehydroxylization behaviors, as discussed above, shown in sol–gel and precipitated samples are different. At the same calcination temperature the structural distortion caused by the insertion of OH^- in the structure is more important. The precipitated sample retailed more hydroxyls in its structure compared to sol–gel one, which is supported by the crystalline structure refinements, its lattice cell distortion is hence bigger. Particularly, the retailed hydroxyls in the network of precipitated sample produces significant influence on the crystalline structure above 600°C since the additional effect of the calcination temperature, resulting in a stronger structural distortion.

In each sample, tetragonal and monoclinic crystals coexisted. Their concentrations changed with the

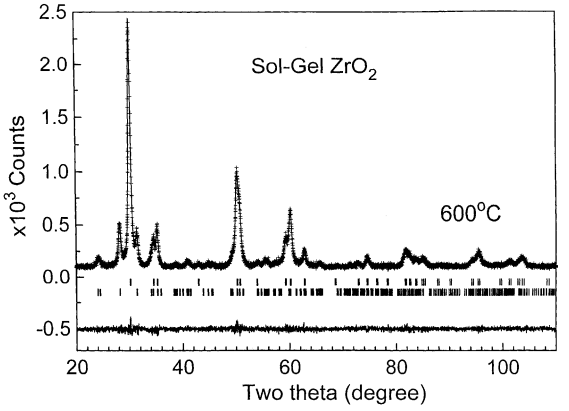

Fig. 8. Rietveld refinement plot of the precipitation zirconia sample calcined at 600°C. The solid continuous line is the calculated pattern while the crosses are the experimental data. The upper line marks correspond to tetragonal phase and the lower line marks correspond to monoclinic phase. The lowest line is the difference between the calculated and experimental data.

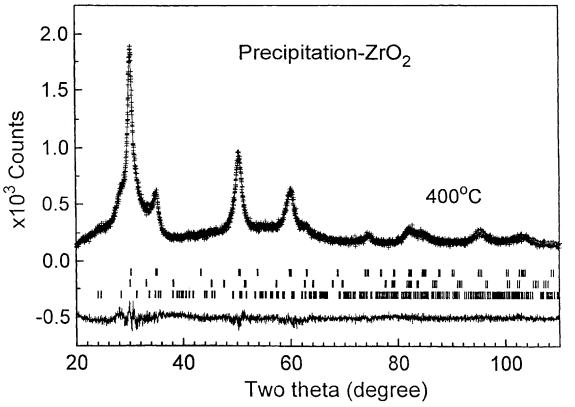

Fig. 10. Rietveld refinement plot of the precipitation zirconia sample calcined at 400°C. The experimental data were fitted with three phases. The upper line marks correspond to tetragonal phase; the middle marks correspond to pseudo-tetragonal and the lower line marks correspond to monoclinic phase.

Table 4
Lattice cell parameters of the tetragonal phase as a function of annealing temperature

Temperature (°C)	Precipitation		Sol–gel	
	a (nm)	*c* (nm)	*a* (nm)	*c* (nm)
400	0.3607 (2)	0.5130 (7)	0.35952 (4)	0.51742 (9)
600	0.35940 (5)	0.5165 (1)	0.35964 (2)	0.51845 (5)
800	0.35644 (5)	0.5176 (1)	0.35961 (3)	0.51908 (9)

Table 5
Lattice cell parameters of the monoclinic phase as a function of annealing temperature

Temperature (°C)	Precipitation			Sol–gel		
	a (nm)	*b* (nm)	*c* (nm)	*a* (nm)	*b* (nm)	*c* (nm)
400	0.5118 (9)	0.5149 (8)	0.5370 (6)	0.515 (1)	0.518 (1)	0.532 (1)
600	0.5275 (2)	0.5219 (2)	0.51151 (2)	0.5145 (2)	0.5197 (2)	0.5316 (2)
800	0.5144 (7)	0.51964 (8)	0.53108 (8)	0.51462 (3)	0.52013 (4)	0.53180 (4)

annealing temperature (Table 6). At 400°C the main phase is tetragonal, but when the temperature was increased, the tetragonal phase concentration decreased with an increase in concentration of monoclinic phase. At 800°C the monoclinic phase concentration was more than 80 wt.%, which is different from the other reports where the low-temperature monoclinic phase transforms to the tetragonal one and then into cubic phase at much higher temperature [25]. In our cases, whatever the samples were prepared in an acidic or base media and whatever the preparation method is sol–gel or precipitation, the samples contain both tetragonal and monoclinic without cubic phase and phase transformation from tetragonal to monoclinic irreversibly occurs when they are calcined.

It is noteworthy that for the precipitation sample calcined at 400°C, when only a tetragonal and a monoclinic structure were modeled to fit the experimental data, the refinement showed a large residual crystals (Fig. 9). This indicated that another phase not included in our model coexisted with them. When we added to our model structure another tetragonal phase with a very small average crystallite size, a good fitting of the calculated data to experimental one was obtained (Fig. 10). It is well known that the freshly derived zirconium gels of the precipitation samples are amorphous and have a solid skeleton that contains many hydroxyls. During annealing, surface hydroxyls condensation causes the nucleation of new oxide crystals and the growth of the existing ones. The TG analysis showed that these gels underwent a continuous weight loss between 200 and 400°C that corresponded to the dehydroxylation of the zirconyl clusters and its transformation into ZrO_2. The formation of the almost amorphous tetragonal phase is probably associated with this process. Since during the precipitation procedure, many extra water molecules and hydroxyl ions linked to the sample that could produce inhomogeneous phases, the quasi-amorphous tetragonal phase could be associated to the sample

Table 6
Phase concentration (wt.%) as a function of annealing temperature

Temperature (°C)	Precipitation			Sol–gel	
	Tetragonal	Quasi-amorphous	Monoclinic	Tetragonal	Monoclinic
400	30 (2)	38 (2)	32 (10)	84 (6)	16 (5)
600	48 (4)		52 (10)	59.2 (1)	41 (9)
800	17 (7)		83 (4)	11.9 (7)	88 (5)

Table 7
Average crystallite size (nm) as a function of annealing temperature

Temperature (°C)	Precipitation			Sol–gel	
	Tetragonal	Quasi-amorphous	Monoclinic	Tetragonal	Monoclinic
400	16 (2)	1.7 (1)	6 (1)	11.9 (7)	10 (3)
600	14 (1)		7 (1)	22.3 (9)	26 (4)
800	12 (3)		18 (1)	36 (1)	30 (5)

regions rich in hydroxyls and water, which should produce cationic vacancies in it.

On the other hand, for the sol–gel sample calcined at 400°C, we obtained a satisfactory fit between the experimental and calculated data when only one tetragonal and one monoclinic phases were used to model the diffraction pattern. This is because the sol–gel sample was more homogeneous than the precipitated one. In the sol–gel method hydroxyl ions are homogeneously distributed in the whole sample. Therefore, quasi-amorphous tetragonal phase was not formed in the sol–gel sample.

Both, the tetragonal and monoclinic phases were nanocrystalline when they were calcined between 400 and 800°C, with an average crystallite size ranging from 6 to 36 nm (Table 7). To our surprise, compared with the sol–gel sample, the average crystallite size of both tetragonal and monoclinic phases in the precipitated sample were much less than that in sol–gel samples, which are only half or one-third smaller than the sol–gel crystals when the samples were heated at 800°C for 4 h, indicating that the crystals of the precipitation sample have higher stability and resist sintering. This result is valuable because it shows that by the precipitation thermal-resistant nanocrystalline zirconia can be produced at a low cost.

It was found that the average crystallite size of the tetragonal phase in precipitated sample slightly decreased as calcination temperature increased. However the same behavior was not observed in the sol–gel samples. Though we did not find a satisfied interpretation for this, it is suggested related to preparation method that results in different phase compositions and crystalline size distributions. As we have mentioned above, due to more hydroxyls retaining in the crystalline network of the precipitation sample, it contains an additional phase (quasi-tetragonal with very fine crystals of about 1.7 nm) at 400°C. However, in the sol–gel the hydroxyl ions are homogeneously distributed in the structures. Therefore, when these samples were calcined, their dehydroxylation behavior and phase transformation thus crystal grain varied from one to another. The precipitated sample contained a relatively larger crystals (16 nm) and very small crystals (1.7 nm) of tetragonal phases at 400°C, when it calcined at a higher temperature 400°C, on the one hand, the quasi-tetragonal phase transformed to tetragonal, this may cause the very fine crystals disappearance; on the other hand, the larger crystals of tetragonal might split into smaller one and it also transferred to monoclinic phase. Finally these complex factors led to a slightly reduction in diameter of tetragonal crystals at 600 or 800°C. Since the sol–gel sample did not exist such a complex phase transformations as occurring in precipitated one and the dehydroxylation process was undergone with a uniform mechanism, its crystal size only showed an increase with the calcination temperature.

3.3. Cationic and anionic defects in lattice

By refining the atomic occupancies in the unit cell, it was found that both the tetragonal and monoclinic structures were cationic or anionic deficient (Tables 8 and 9). Zirconium occupancy numbers were smaller than the ideal values of 0.125 for the tetragonal phase and 1.0 for monoclinic one for the precipitation

Table 8
Zirconium lattice vacancies in the monoclinic structures[a]

Annealing temperature (°C)	Precipitation			Sol–gel		
	O_{az}	C_{dz}	N_{dz}	O_{az}	C_{dz}	N_{dz}
600	0.83 (2)	17	0.68	0.59 (7)	41	1.6
800	0.85 (2)	15	0.60	0.87 (3)	14	0.56

[a] O_{az}: zirconium atomic occupancy; C_{dz}: concentration of zirconium vacancies in unit cell; N_{dz}: number of zirconium vacancies in unit cell.

Table 9
Zirconium and oxygen atomic vacancies in the tetragonal structures[a]

Annealing temperature (°C)	Precipitation			Sol–gel		
	O_{az}	C_{dz}	N_{dz}	O_{ao}	C_{do}	N_{do}
600	0.085 (2)	32.0	1.28	0.244 (2)	2.4	0.2
800	0.119 (6)	4.8	0.19	0.215 (3)	14	1.1

[a] O_{az}: zirconium atomic occupancy; C_{dz}: concentration of zirconium vacancies in unit cell; N_{dz}: number of zirconium vacancies in unit cell. O_{ao}: oxygen atomic occupancy; C_{do}: concentration of oxygen vacancies in unit cell; N_{do}: number of oxygen vacancies in unit cell.

samples. This clearly shows that cationic defects are formed in the crystalline structures of zirconia phases. For the monoclinic phases in both synthesis methods, the zirconium defects concentration decreased when the annealing temperature increased from 600 to 800°C. In opposition, the tetragonal structure of the sol–gel samples calcined at 600 and 800°C were deficient in oxygen with a concentration that increased as the annealing temperature was raised. In the tetragonal phase of the precipitated sample the deficiency was cationic and its concentration decreased as the annealing temperature increased. These results strongly indicate that the forming mechanisms of atomic defects in the monoclinic and tetragonal structures are different.

The formation of the cationic defects in the crystalline structure is reported to be associated with the hydroxyl ions inserted in the lattice sites [26,27]. When the sample was prepared, in the stage of hydrolysis, some hydroxyl ions linked the framework of the Zr–O structure and replaced some oxygen lattices, generating the extra positive charges. This must produce some cationic defects to balance the extra positive charges and remain electron neutrality in the crystal as a whole. Because most of those OH^- ions left the surface and the structural network when the sample was calcined at high temperature, the concentration of cationic defects therefore diminished. This reasonably explains the variation of cationic defects with annealing temperature.

It is easy to understand the generation of oxygen defects in the crystalline structures of tetragonal crystals in the sol–gel samples. When the sample was calcined, the hydroxyls retailed in the structure left it to form molecular water, releasing the lattice oxygen (O_L^{2-}), and producing an oxygen defect (V_o) in its position:

$$O_L^{2-} \cdots H^+ + H^+ \cdots O_L^{2-} \rightarrow H_2O + O_L^{2-} + V_o^{\bullet\bullet} \quad (6)$$

The high-temperature annealing favors the removal of hydroxyls producing more oxygen defects. This result shows that the dehydroxylation of the tetragonal phase prepared with sol–gel technique is easier than precipitated sample. The different dehydroxylation behaviors are generally related to the preparation methods. The interaction between the inserting hydroxyl ions and lattice sites is more stronger in the precipitated sample than that in the sol–gel one, this delays the hydroxyls inserting in the structural network removing at a temperature higher than 800°C for the precipitated sample. That is why oxygen defects were not created in the tetragonal phase in this sample at 800°C.

4. Conclusions

Nanocrystalline zirconia can be synthesized by using the precipitation method with low cost precursors. It has a higher thermal resistance than that prepared with sol–gel method. In both precipitation and sol–gel samples, the tetragonal and monoclinic nanophases coexist. The tetragonal phase, however, irreversibly transformed into monoclinic zirconia when the samples were annealed at temperatures higher than 400°C. The inhomogeneity of the precipitated sample gave rise to quasi-amorphous tetragonal zirconia at 400°C. This phase retains a lot of hydroxyls in its crystalline producing many cationic defects.

The crystalline structure of the monoclinic zirconia had also cationic defects, which had concentrations that increased with the annealing temperature, independently of the synthesis method. On the contrary, in the structure of tetragonal zirconia, the type of vacancies depended on the preparation technique. Zirconium vacancies occurred in the precipitation sample, and its number decreased when the annealing temperature increased, but oxygen vacancies were created in those prepared by the sol–gel method; its concentration increased as the calcination temperature was increased.

Acknowledgements

J.A. Wang would like to acknowledge the financial support from the projects FIES-98-29-III (IMP-IPN-Mexico) and CONACY-99-31282-U (Mexico) and CGEPI-99-130 (IPN-Mexico). The authors also thank Mr. M. Aguilar for XRD data collection and Mr. A. Morales for sol–gel sample preparation.

References

[1] K. Tanabe, T. Yamaguchi, Stud. Surf. Sci. Catal. 44 (1989) 99.
[2] K. Tanabe Misono, M. Ono, H. Hattori, Stud. Surf. Sci. Catal. 51 (1989) 199.
[3] B.H. Davis, R.A. Keogh, R. Srinivasan, Catal. Today 20 (1994) 219.
[4] A. Corma, Chem. Rev. 95 (1995) 559.
[5] X. Song, A. Sayari, Catal. Rev.-Sci. Eng. 38 (1996) 329.
[6] K. Arata, Adv. Catal. 37 (1990) 165.
[7] K. Arata, M. Hino, Mater. Chem. Phys. 26 (1990) 213.
[8] K. Arata, Trends Phys. Chem. 2 (1991) 1.
[9] C. Morterra, G. Cerrato, C. Emanuel, V. Bolis, J. Catal. 142 (1993) 349.
[10] D. Farcasiu, J.Q. Li, Appl. Catal. A 128 (1995) 97.
[11] C. Li, P.C. Stair, Catal. Lett. 36 (1996) 119.
[12] D. Spielbauer, G.A.H. Mekhemer, E. Bosh, H. Knözinger, Catal. Lett. 36 (1996) 59.
[13] H. Liu, V. Adeeva, G.D. Lei, W.M.H. Sachtler, J. Mol. Catal. A 100 (1995) 35.
[14] R.A. Comelli, S.A. Canavese, S.R. Vaudagna, N.S. Figoli, Appl. Catal. A 135 (1996) 287.
[15] S.L. Soled, E. Iglesia, G.M. Kramer, Stud. Surf. Sci. Catal. 90 (1994) 531.
[16] C. Miao, W. Hua, J. Chen, Z. Gao, Catal. Lett. 37 (1996) 187.
[17] C.T. Young, J.D. Bode, Paper No. 790143, SAE Congress, Detroit, February 1979.
[18] E.C. Subbarao, H.S. Maiti, Adv. Ceram. 24 (1998) 731.
[19] C.B. Alcock, Mater. Sci. Res. 10 (1975) 419.
[20] E.C. Subbarao (Ed.), Solid Electrolytes and Their Applications, Plenum Press, New York, 1980.
[21] W.P. Dow, Y.P. Wang, T.J. Huang, J. Catal. 160 (1996) 155.
[22] R. Gómez, T. López, X. Bokhimi, E. Moñoz, J.L. Boldú, O. Novaro, Sol–Gel Sci. Technol. 11 (1998) 309.
[23] X. Bokhimi, A. Morales, O. Novaro, M. Portilla, T. López, F. Tzompantzi, R. Gómez, J. Sol. State Chem. 135 (1998) 28.
[24] M. Maczka, E.T.G. Lutz, H.J. Verbeek, K. Oskam, A. Meijerink, J. Hanuza, M. Stuivinga, J. Phys. Chem. Solid 60 (1999) 1909.
[25] M. Yoshimura, Am. Ceram. Soc. Bull. 67 (1998) 1950.
[26] J.A. Wang, X. Bokhimi, O. Novaro, T. López, R. Gómez, J. Phys. Chem. B 103 (1999) 299.
[27] J.A. Wang, X. Bokhimi, O. Novaro, T. López, R. Gómez, J. Mol. Catal. A 137 (1999) 139.